Carbohydrate Polymer Technologies and Applications 10 (2025) 100709

Contents lists available at ScienceDirect

Carbohydrate Polymer Technologies and Applications

journal homepage: www.sciencedirect.com/journal/carbohydrate-polymer-technologies-and-applications

Aloe barbadensis polymeric acetylated mannan modified by self-assembly through a pervaporation aloe polysaccharide membrane: Safety evaluation and tail fin regeneration in zebrafish

Di Li [a,1], Jiajie Deng [b,1], Mengmeng Wang [a,1], Haiyang Yin [a], Jinzi Chen [a], Weijie Xu [a], Xiaofeng Guo [a], Xueli Tong [a], Ding Ye [c,*], Jiejing Li [a,d,*]

[a] Department of Research & Development Guangzhou Oriplamacy Technology Co, Ltd. Guangzhou, Guangdong 510000, China
[b] National Aquatic Biological Resource Center Institute of Hydrobiology, Chinese Academy of Sciences Wuhan, Hubei 430072, China
[c] School of Marine Biology and Fisheries, Hainan University, Haikou, Hainan 570228, China
[d] Guangdong Provincial Key Laboratory of Drug Non-Clinical Evaluation and Research, Ltd. Guangzhou, Guangdong 510980, China

ARTICLE INFO

Keywords:
Synthetic polysaccharide polymer
Membrane pervaporation
Hydrophobic-hydrophilic polysaccharide
Wound healing
Macrophage
Anti-inflammation
Mitochondrial biogenesis

ABSTRACT

Aloe vera has a remarkable anti-inflammation effect in wound healing and other skin disorders. Its bioactivity is mainly attributed to the polysaccharides. However, the clinical applications of aloe vera are considerably restricted by the low efficacy of its extracts. To increase its bioactivity, it is necessary to develop de novo techniques for extracting and modifying aloe polysaccharides. This study used pervaporation to perform self-assembly of aloe vera polysaccharides, leading to the production of aloe barbadensis polymeric acemannan 2 (ABPA2). ABPA2 was associated with increasing of acytel functional groups compared to ABPA1. Electron microscopic analysis showed ABPA2 was able to form supporting membrane. The safety of ABPA2 was evaluated through acute and chronic toxicity experiments. Functionally, it was able to induce zebrafish tail fin healing after wounding. The effects were in all likelihood ascribed to its ability to induce proliferation and macrophage extravasation in wounded tail fin. By applying RNA-seq, it showed that ABPA2 triggered multiple types of cells differentiated and proliferation mainly through regulating genes expression of extracellular matrix. After all it was able to activate mitochondrial biogenesis through regulating mechanotransduction of calcium. These findings warrant a further chemical-biological investigation in mammalian wound healing.

Abbreviations

AVBEC	aloe vera barbadensis extract C
ABPA1	aloe barbadensis polymeric acemannan 1
ABPA2	aloe barbadensis polymeric acemannan 2
GC–MS	gas chromatography-mass spectrometer
HPGPC	high-performance gel permeation chromatography
HE	hematoxylin eosin
NMR	nuclear magnetic resonance
OXPHOS	oxidative phosphorylation
TCA	tricarboxylic acid
ALT	alanine transaminase
AST	aspartate transaminase
ALP	alkaline phosphatase
CK	creatine kinase
CRE	creatinine
TBIL	total bilirubin
GGT	γ-glutamyltransferase
ALB	albumin
TP	total protein
UREA	urea nitrogen
CHOL	total cholesterol
GLU	glucose
TG	triglycerides
PRO	protein
OB	occult blood
KET	ketone bodies
BIL	bilirubin

* Corresponding authors.
E-mail addresses: 996996@hainanu.edu.cn (D. Ye), xenjiejingli@gmail.com (J. Li).
[1] Co-first authors: Di Li, Jiajie Deng, Mengmeng Wang

https://doi.org/10.1016/j.carpta.2025.100709

Available online 13 February 2025

URO	urobilinogen
SG	specific gravity
WBC	white blood cells
NIT	nitrite
NEUT	neutrophil
LYM	lymphocyte
MONO	monocyte
EOS	eosinophil
BASO	basophil
RBC	red blood cell count
HGB	hemoglobin
HCT	hematocrit level
MCV	mean corpuscular volume
MCH	mean corpuscular hemoglobin
MCHC	mean corpuscular hemoglobin concentration
PLT	platelet
RETIC	reticulocyte
PT	prothrombin time
APTT	activated partial thromboplastin time
SEM	scanning electron microscopy
PCA	principal component analysis
GO	Gene Ontology
TNF-α	tumor necrosis factor-α
IL-1	interleukin-1
IL-8	interleukin-8
ROS	reactive oxygen species

1. Introduction

Aloe vera (L.) Burm. f. (synonym *Aloe barbadensis Mill.*) is one of the few herbs widely acknowledged and used in Western cultures as well as alternative and complementary remedies in Asia (Hamman, 2008; Minjares-Fuentes et al., 2018). Modern pharmacology studies have shown that aloe vera exerts diverse bioactivities, including anti-tumor, anti-inflammation, immunomodulator, wound repair, and ameliorator of metabolic diseases (Catalano et al., 2024; Cock, 2015; Kumar et al., 2019; Sahebnasagh et al., 2022; Sánchez et al., 2020; Tornero-Martínez et al., 2022). Nonetheless, the clinical application of aloe vera is constrained despite its widespread use in the food and cosmetic industries (Chelu et al., 2023; K & Q, 2004).

The various benefits of aloe vera for the skin are the main reason for its worldwide fame and they are empirically based. Over the past 30 years, systematic research on aloe vera, such as its composition, bioactivity and clinical effectiveness, has increased rapidly. Studies have shown that aloe polysaccharides can promote wound repair by modulating the anti-inflammation, proliferative stages or immunomodulation of the wound repair process (Liang et al., 2021a; Liu et al., 2019; Mr et al., 2014; Xing et al., 2015). Moreover, the effectiveness of aloe vera for various skin disorders, including burn, acute and chronic wounds, has been confirmed in clinical trials (Hekmatpou et al., 2019; Huang et al., 2024; Liang et al., 2021b; Sharma et al., 2022). However, some conflicting results have also been reported. There are a few systematic reviews or meta-analyses of clinical trials have shown that aloe vera has no beneficial effect on skin disorders (Kloter et al., 2023). It can be attributed to its food origin and preparation process rather than its uncertain bioactivity. However, how biological activity is affected by these factors remains unclear.

This study started by producing a crude aloe vera extract, AVBEC (Tong et al., 2021a). Interestingly, it was found that AVBEC produced a highly selective apoptotic effect in tumor cells. The tumoricidal function can be ascribed to adaptive modulation of mitochondrial metabolism (Tong et al., 2021b). Subsequently, a homogeneous polysaccharide (aloe barbadensis polymeric acemannan, ABPA1) was successfully isolated from AVBEC. Next, previous studies confirmed the antitumor activity and immunomodulatory activity of ABPA1 in vitro and in vivo. ABPA1 induced apoptosis in colorectal cancer cells (RKO and SW480) via modulating the tricarboxylic acid cycle (TCA cycle) and oxidative phosphorylation (OXPHOS) (X et al., 2022). Meanwhile, ABPA1 polarized macrophages to a phagocytic phenotype, closely associated with regulating mitochondrial metabolism. Therefore, ABPA1 exhibited activity of anti-inflammation by alleviating macrophage-associated cytokine storm of pneumonia (Li et al., 2022).

Wound healing is a highly coordinated and tightly regulated dynamic process involving the synergistic and integrated actions of cells and cells, cells and intercellular factors cells, and the microenvironment. As a result of tissue ischaemia, inadequate oxygen supply and nutrient deprivation, cells resident in the tissue or recruited from the wound edges must adjust their metabolism to adapt to the changing environment. Thus, it deserves to expand the investigation of ABPA1 into the systematically intricate wound healing process. Unfortunately, no definite phenotype was observed. It could largely due to poor solubility and digestibility of ABPA1. It is therefore unable to be easily taken up by other cell types other than macrophages. Because macrophages are able to take in the polysaccharide by phagocytosis.

It therefore a synthetic polysaccharide was obtained by membrane pervaporation from aloe polysaccharide. Then, using high-performance gel permeation chromatography (HPGPC), Fourier infrared spectroscopy (FTIR), and nuclear magnetic resonance (NMR) spectroscopy, the fabricated pervaporational membrane was identified as a new synthetic polysaccharide polymer different from ABPA1 (aloe barbadensis polymeric acemannan 2, ABPA2). High Hydroxylation were found in the synthetic polysaccharide and therefore it is hydrophilic. At the same time, their carbon chain portion and acetylation are non-polar which make them hydrophobic. Hydrophobic and hydrophilic property eased cellular uptake to allow regulating many cell types other than macrophage.

The aim of this study was to obtain safety information about ABPA2 and preliminarily research its wound healing effect. Therefore, acute and chronic (six-month) toxicity assessments were promptly conducted to determine the need for further investigation. The safety evaluation revealed that ABPA2 is a safe product. Similarly to ABPA1, the regenerative capacity of ABPA2 was evaluated on the zebrafish caudal fin injury model, a rapid screening model. More interestingly, it demonstrated a definite function of ABPA2 to facilitate wound healing in zebrafish. The EdU assay indicated that cell proliferation was notably promoted with ABPA2 treatment. The regulation of acute post-injury inflammation by ABPA2 was confirmed by the migration of immune cells and the levels of inflammatory factors detected. Gene-concept network and GO-MF analysis from RNA-seq analysis demonstrated that the genes were enriched in signaling pathways for extracellular matrix and skeletal reconstruction. Based on the above studies, the necessity of acetyl group for wound healing was demonstrated.

2. Materials and methods

2.1. Isolation, purification, and structural analysis of ABPA2

The preparation of AVBEC has been described in a previous article (Tong et al., 2021c). Additionally, the structure of the homogeneous polysaccharide (ABPA1) isolated from AVBEC has been reported (X et al., 2022). In this study, 100±2 g ABPA1 was dissolved in 10 L of 20 % ethanol solution and evaporated the solvent at a constant temperature of 80 °C using a 20 L stainless steel open evaporation tank (MC-JSF-20 L, MC-biolab, China), resulting in the formation of a polysaccharide membrane on the surface of the solution. Polysaccharide membranes were collected every 8 h until no polysaccharide membranes formed. During the process of collecting the membranes, no stirring is carried out. In general, it can be collected 3–4 times. Each batch of polysaccharide membranes collected was weighed (wet weight) and tested for total solids and O-acetyl content (Table S1). The weight difference was used to calculate solid content. Polysaccharide O-acetyl content was crude assesses with acetylcholine chloride standards (CCAD301227,

CATO). After that, all the collected polysaccharide membranes are combined together and purified according to previously published methods. Another purified polysaccharide (ABPA2) was obtained. In the process of repeated preparation, the yield of ABPA2 from ABPA1 was approximately 1 ‰.

The structure of ABPA2 was characterized using HPGPC (LC-10A, Shimadzu, Japan), gas chromatography-mass spectrometer (GC–MS, Agilent, 7890A and 5977B, respectively, Agilent Technologies, USA), ion chromatography (IC, ICS5000, Thermo, USA), Fourier infrared spectroscopy (FTIR, Nicolet 6700, Thermo, USA), and nuclear magnetic resonance spectroscopy (NMR, Bruker AVANCE HD III 600 MHz spectrometer, Bruker, Germany) based on established methods (X et al., 2022).

2.2. Experimental animals

Sprague Dawley (SD) rats were acquired from the Hunan Slack Jingda experimental animal Co., Ltd. (SCXK [Xiang] 2019–0004). All rats were housed in the animal facility with a 12 h dark and 12 h light cycle, 40 %–70 % humidity, and 22 ± 2 °C temperature (SYXK [Guangdong] 2018–0014). All animals were quarantined and raised for five days to adapt to the altered conditions. The rats were numbered with 2 % Silver nitrate solution (coffee-colored, indicate ten digits) and 2 % gentian violet solution (purple, indicate single digits) before the experiments. All experimental procedures followed the ARRIVE guidelines (http://www.nc3rs.org.uk/arrive) and were authorized by the Institutional Animal Care and Use Committee of the Sci-tech Industrial Park, Guangzhou University of Chinese Medicine. The approval numbers for acute and chronic toxicity studies were PZ21054 and PZ21055, respectively. Due to the evident difference in the appearance of ABAP2 and water, the experimenter cannot be blinded to the grouping. However, except for histopathological analysis, all other data are provided by the instrument to provide unbiased analysis. In the safety evaluation experiments, none of the analyses revealed a sex difference; hence, the histopathological examination data for each sex was combined.

Wildtype zebrafish of the AB strain, *Tg2(mpeg: EGFP)* and *Tg(lyz: DsRed2),* were obtained from the China Zebrafish Resource Center (http://zfish.cn). The zebrafish experiments were performed according to the National Institute of Health (National Research Council) Guide for the Care and Use of Laboratory Animals, with the approval of the Institutional Animal Care and Use Committee of the Institute of Hydrobiology, Chinese Academy of Sciences (Approval number: E1490301). This study used female and male zebrafish, and the data revealed no significant gender differences.

2.3. Safety evaluation of ABPA2 in SD rats

2.3.1. Acute toxicity study

For the acute oral toxicity study, 24 SD (SPF level) rats (7–8 weeks old), half male and half female, were acquired. After a five-day adaptation feeding period, female rats exhibited a weight range of 192.1–208.9 g, with an average weight of 199.4 g, and male rats displayed a weight range of 193.4–205.4 g, with an average weight of 199.2 g. The body weights of both male and female rats remained within 20 % of their respective average weights. Using a random number table generated in Excel, 20 SD rats were randomly selected for subsequent experiments. The experimental design comprised two groups: The negative control group, which received purified water, and the ABPA2 group, which received ABPA2, and the animals were stratified based on sex and body weight. Within each stratum, rats were randomly divided into two groups (n = 10, half male and half female).

Given the low toxicity and biocompatibility of polysaccharides, the maximum feasible dose (MFD) of the test substance was used to evaluate the toxicological response to ABPA2 in rats. Due to the limited solubility of ABPA2 in water, 1 g of ABPA2 was dissolved in 4 mL of water. Furthermore, according to the China Food and Drug Administration guidelines (20,140,513), the maximum volume tolerable by SD rats is 20 mL/kg. The acute toxicity test allows for administering multiple doses in a single day. Consequently, the rats in the two experimental groups were administered doses of either ABPA2 or water at a rate of 20 mL/kg (5g/kg) three times during a 24-h period, with an interval of at least four h between each administration. The day the rats were exposed to ABPA2 or water was recorded as D0. General health observations (daily), mortality (daily), weight (once a week), and symptoms of poisoning (daily) were monitored and registered for two weeks. The two-week posttreatment observation period was recorded as oD1 to oD14 (observation period). The rats were sacrificed and examined for histopathological changes at oD14.

2.3.2. Six-month chronic toxicity study

For the chronic oral toxicity study, 66 SD rats (6–7 weeks old), half male and half female, were acquired. After a five-day adaptation feeding period, three lower-weight rats were separated from each sex. Female rats weighed 170.0–215.3 g, with an average weight of 194.8 g, while male rats weighed 204.9–243.1 g, with an average weight of 222.4 g. The body weights of both male and female rats remained within 20 % of their respective average weights. The experimental design comprised two groups: The negative control group, which received purified water, and the ABPA2 group, which received ABPA2, with the animals stratified by sex and body weight. Within each stratum, rats were randomly allocated to the two groups (n = 30, half male and half female).

As no mortality was recorded during the acute toxicity study, the dosage in the following long-term toxicity experiments was set at 1 g/kg/day (1/15 of the MFD in the acute toxicity study). The rats were given these experimental treatments every morning for six months, and the corresponding period was recorded as D1–D181. Additionally, a four-week recovery period after the final administration was recorded as rD1 to rD29. General health observations were conducted daily, and the weights and food intakes for each rat were recorded once per week. The volume of ABPA2 was adjusted once per week according to the weights of the rats. At the mid-term administration period (D90), 10 rats (half of each sex) from each group fasted for 12 h, and their urine samples were collected. The next day (D91), they were sacrificed, and three blood samples were collected from the abdominal aorta for hematological analysis (EDTA-K2 tubes), biochemistry analysis (dry tubes), and coagulation tests (sodium citrate tubes). Vital organs, including the heart, liver, and kidney, were excised, weighed, and fixed in 10 % formaldehyde, while the testis was fixed in Davidson fixative solution for histopathological examination after euthanasia. The femur marrow was used for the bone marrow smear. Similarly, urine was collected from the remaining 20 rats in each group at the end of the administration period (D181) and on the last day of the recovery period (rD28). The rats were sacrificed on the first day of the recovery period (rD1, 20 rats) and at the end of the recovery period (rD29, 20 rats).

For the biochemistry analysis, blood samples were collected in dry tubes and placed in a constant-temperature tank at 37 °C for 30 min. Then, the samples were centrifuged at 3000 rpm for 10 min, and the 100 uL supernatant was carefully transferred to another cleaning tube. Alanine transaminase (ALT), aspartate transaminase (AST), alkaline phosphatase (ALP), creatine kinase (CK), creatinine (CRE), total bilirubin (TBIL), γ-glutamyltransferase (GGT), albumin (ALB), total protein (TP), urea nitrogen (urea), total cholesterol (CHOL), glucose (GLU), and triglycerides (TG) were detected using a Hitachi 7080 analyzer, while potassium (K^+), sodium (Na^+), and chloride (Cl^-) were detected using a MEDICA Easylyte analyzer (MEDICA, USA).

Urine samples were collected using stress stimulation. Glucose (GLU), protein (PRO), pH, occult blood (OB), ketone bodies (KET), bilirubin (BIL), urobilinogen (URO), specific gravity (SG), white blood cells (WBC), and nitrite (NIT) were detected by CLINITEK100 (BAYER, Germany).

For the hematological analysis, the samples were collected in EDTA-

K2 tubes and analyzed within 30 min. The white blood cell count (WBC), neutrophil ratio (%NEUT), lymphocyte ratio (%LYM), monocyte ratio (%MONO), eosinophil ratio (%EOS), basophil ratio (%BASO), red blood cell count (RBC), hemoglobin (HGB), hematocrit level (HCT), mean corpuscular volume (MCV), mean corpuscular hemoglobin (MCH), mean corpuscular hemoglobin concentration (MCHC), platelet count (PLT), and reticulocyte ratio (%RETIC) were examined using an ADVIA2120 automatic cell analyzer (Siemens, Germany). Samples collected in sodium citrate-containing tubes were used for the coagulation test. The prothrombin time (PT) and activated partial thromboplastin time (APTT) were measured using a Sysmex CA1500 (SYSMEX, Japan).

The fixed organs were dehydrated in gradient ethanol, vitrified, and embedded in paraffin. Sections (5 μm thick) were cut with an RM2235 microtome (Leica, Germany) and stained with hematoxylin and eosin. Bone marrow from the femur was smeared. Histological observations were performed using a Leica DMLB bright field microscope (Leica, Germany) at 200 and 400 magnification to evaluate the degree of pathological alteration.

2.3.3. Preparation of the subject sample

The subject sample were prepared fresh one day in advance. A sufficient amount of ABPA2 was weighted into a Schott bottle according to the designed gavage dose and dissolved to the appropriate volume with purified water. The flask was kept overnight under stirring at 37 °C to ensure the sample completely dissolved. The next day, volumes of polysaccharide solution were calculated according to the body weight of each rat. After that, the dose via intragastric gavage was adjusted weekly according to the body weight of rats.

2.4. Determination of the safe concentration of ABPA2 in zebrafish

Improper drug concentrations can lead to toxic side effects in organisms. Therefore, when conducting drug experiments on zebrafish, it is essential first to determine a range of drug concentrations that are relatively non-toxic, allowing for the selection of effective drug concentrations without harming the survival of the zebrafish. For ABPA2, six concentration gradients were designed. The results revealed that at a drug concentration of 0.05 %, the mortality rate of the treated zebrafish larvae was 0 %. Accordingly, 0.05 % was selected as the highest concentration for this experiment. To determine the optimal concentration within the safe range for significantly promoting zebrafish tail fin regeneration, four concentrations were designed, including 0.0375 %, 0.01 %, 0.005 %, and 0.001 %. The results demonstrated that 48 and 72 h after tail fin amputation, tail fin lengths in 0.0375 %, 0.005 %, and 0.001 % drug concentration groups were all higher than those in the control group, indicating that these three concentrations can promote tail fin regeneration in zebrafish larvae (Figure S2). At 120 h post-amputation (hpa), only the 0.0375 % group exhibited a significantly longer tail fin than the control group, suggesting that among these concentrations, the 0.0375 % drug treatment had the most significant effect on promoting tail fin regeneration. In terms of regeneration speed, the control group reached its peak at 72 h post-amputation, while the 0.0375 % drug concentration group reached its peak at 48 h, with a growth rate from 24 to 48 h, approximately 1.7 times that of the control group (72.2 μm versus 121.8 μm). Therefore, 0.0375 % ABPA2 was the subsequent experimental dosing concentration.

2.5. Caudal fin regeneration assay for larval fish

The 72 hpf zebrafish were first anesthetized with Tricaine. The caudal fin was cut at the caudal tip of the notochord along the dorsoventral axis of the body. Seventy-five fin-clipped fish were randomly divided into two groups: The control group and the ABPA2-treated group. The treatment was performed for five days, and the medium of each group was changed daily. A bright field image was obtained for each fish using a microscope at the same magnification at 0, 24, 48, 72, 96, and 120 hpa. The caudal fin lengths were measured from the posterior tip of the fin fold to the notochord end along the anterior-posterior axis.

2.6. Caudal fin regeneration assay for adult fish

To determine whether ABPA2 can accelerate caudal fin regeneration in adult zebrafish, half of the caudal fin was amputated from 3-month zebrafish, and the fish were treated either with or without ABPA2 for nine days, with the length of the caudal fins measured daily. Bright-field images of each fish were acquired using a stereomicroscope at the same magnification of 1, 3, 5, 7, and 9 days post-amputation (dpa). The color of the newly grown caudal fin was lighter, forming a line at the cutting edge. The length of the regenerated fin was measured from the end of the middle stripe at the cutting side to the posterior tip of the fin fold along the anterior-posterior axis.

2.7. Counting of macrophages and neutrophils at the wounded fin

To count the neutrophils, three dpf Tg (lyz: DsRed2) zebrafish labeling neutrophils were anesthetized with tricaine. The caudal fin was cut in half. Thirty fin-clipped fish were randomly divided into two groups: The control group and the ABPA2-treated group. The treatment was performed for 8 h. A bright field and fluorescent images were acquired for each fish using an inverted microscope under a 10x objective at 0, 3, 6, and 8 hpa.

Three dpf Tg2 (mpeg1: EGFP) zebrafish were used to count macrophages. The same procedures were performed as described above but with a different treatment period. The treatment was performed for four days, and the medium of each group was changed daily. A bright field and fluorescent images were acquired for each fish using an inverted microscope under a 10 x objective at 0, 24, 48, 72, and 96 hpa. The neutrophils and the macrophages at the wound site were counted using the images.

2.8. Cell proliferation assay by EdU labeling

The 72 hpf zebrafish were first anesthetized with Tricaine. The caudal fin was cut at the caudal tip of the notochord along the dorsoventral axis of the body. Thirty fin-clipped fish were randomly divided into two groups: The control group and the ABPA2-treated group. The larval fish were treated with 500 μM EdU for 10 h, fixed with 4 % paraformaldehyde (PFA), neutralized with 2 mg/mL glycine solution for 5 min, then permeated with 2 %Triton X-100 for 2 h. The Yefluor 594 EdU fluorescent staining kit was used to detect cell proliferation signals.

2.9. Sample perpetration and bulk RNA-sequencing

The caudal fins of the 72 hpf zebrafish were cut and treated with or without ABPA2, as described above. At 6 hpa and 36 hpf, fish from the control and ABPA2-treated groups were collected for RNA bulk-seq; 40 fish from each group were collected and divided into two replicates. The RNA was extracted and purified using a total RNA isolation kit (RC112, Vazyme). The quality of RNA was determined by Nanodrop, Qubit, and Labchip GX. For each sample, 100 ng of RNA was used for cDNA synthesis (Discover-sc WTA Kit, N711, Vazyme), and the length distribution of cDNA was tested on Agilent 2100. The cDNA libraries were then constructed using the TruePrep DNA Library Prep Kit (D501, Vazyme). The sequencing was performed on Illumina NextSeq 500 with a read length of 150 bp paired-end at the Analysis and Testing Center of the Institute of Hydrobiology, Chinese Academy of Sciences, China. Around 2 G clean data with Q30 $>$ 90 % were generated for each sample. The clean data were mapped to zebrafish reference transcripts derived from the GRCz11 Ensembl release 97 genome using Bowtie2 with the default parameters. Transcripts were normalized and quantified by RNA-

sequencing (RNA-Seq) by Expectation Maximization. The principal component analysis was performed using the R package. Differential expression analysis was conducted using DEseq2. Genes with |log2-foldchange| > = 1 and adjusted $p < 0.05$ were considered as differentially expressed genes (DEGs) and were used for gene ontology (GO) enrichment analysis. The GO enrichment analysis and the gene concept network were performed by ClusterProfiler 4.0.

2.10. Quantitative PCR validation

Total RNA was extracted using RNA Extraction Kit (Servicebio) according to the manufacturer's instructions. cDNA was obtained from total RNA using HiScript® II Reverse Transcriptase (Vazyme) in 25 μL reactions. Quantitative real-time polymerase chain reaction (qRT-PCR) based on 2 × SYBR Green qPCR Master Mix (G3320, Servicebio, China) was performed using a Real-Time PCR system (CFX, Bio-Rad, USA) (Bustin et al., 2009). β-actin was selected as the reference gene. Quantification of gene expression was calculated by the standard curve and cycle threshold of each sample. The results of genes expression were normalized to reference gene expression.

2.11. Data processing and statistical analyses

The images were processed and measured by Fiji software 28. Statistical analyses were performed using GraphPad Prism (version 8.0) software and presented as mean ± standard deviation from at least three separate experiments. Statistical significance between experimental and control groups was determined by one-way analysis of variance or *t*-test. $p < 0.05$ indicated that the difference between the mean values is statistically significant. Statistical significance is represented by asterisks ($^{*}p < 0.05$, $^{**}p < 0.01$, $^{***}p < 0.001$).

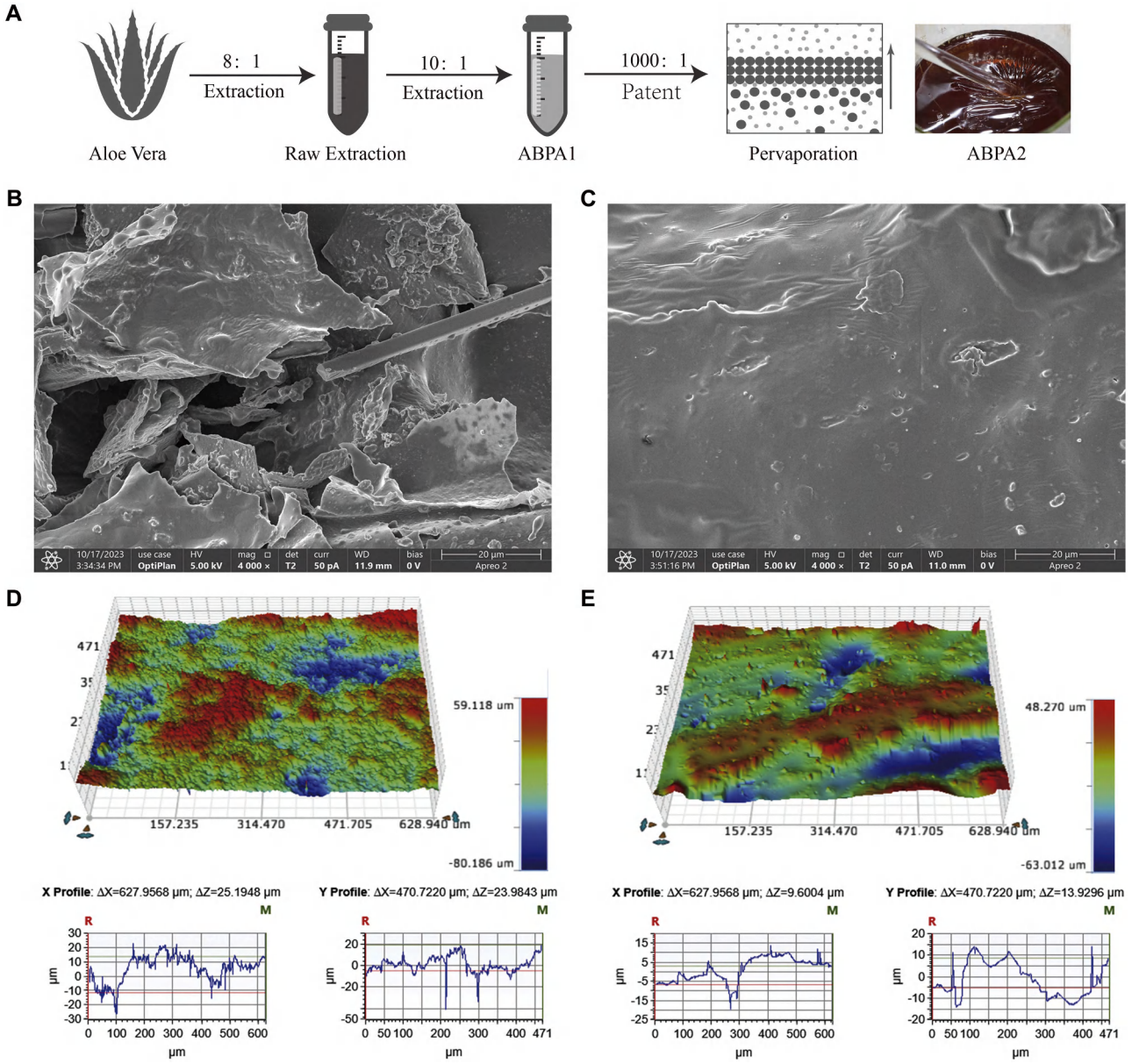

Fig. 1. Isolation and surface characteristics of the two aloe polysaccharides. (A) Flow chart of the separation process of ABPA2. (B) Representative scanning electron microscopy (SEM) image of ABPA1. Original magnification: × 4000. (C) Representative SEM image of ABPA2. Original magnification: × 4000. (D) The surface roughness of ABPA1 under a 3D optical profilometer. (E) The surface roughness of ABPA2 under a 3D optical profilometer.

3. Results

3.1. Structure identification of the ABPA2: High acetylated mannan

The preparation process of aloe vera extract AVBEC and the purification process of ABPA1, the main polysaccharide in AVBEC, have been thoroughly described in previous articles (Tong et al., 2021a; X et al., 2022). Briefly, ABPA1 was obtained from AVBEC by ethanol precipitation and further purification. While the immunomodulatory and anti-tumor activities of ABPA1 has been intensively studied (Li

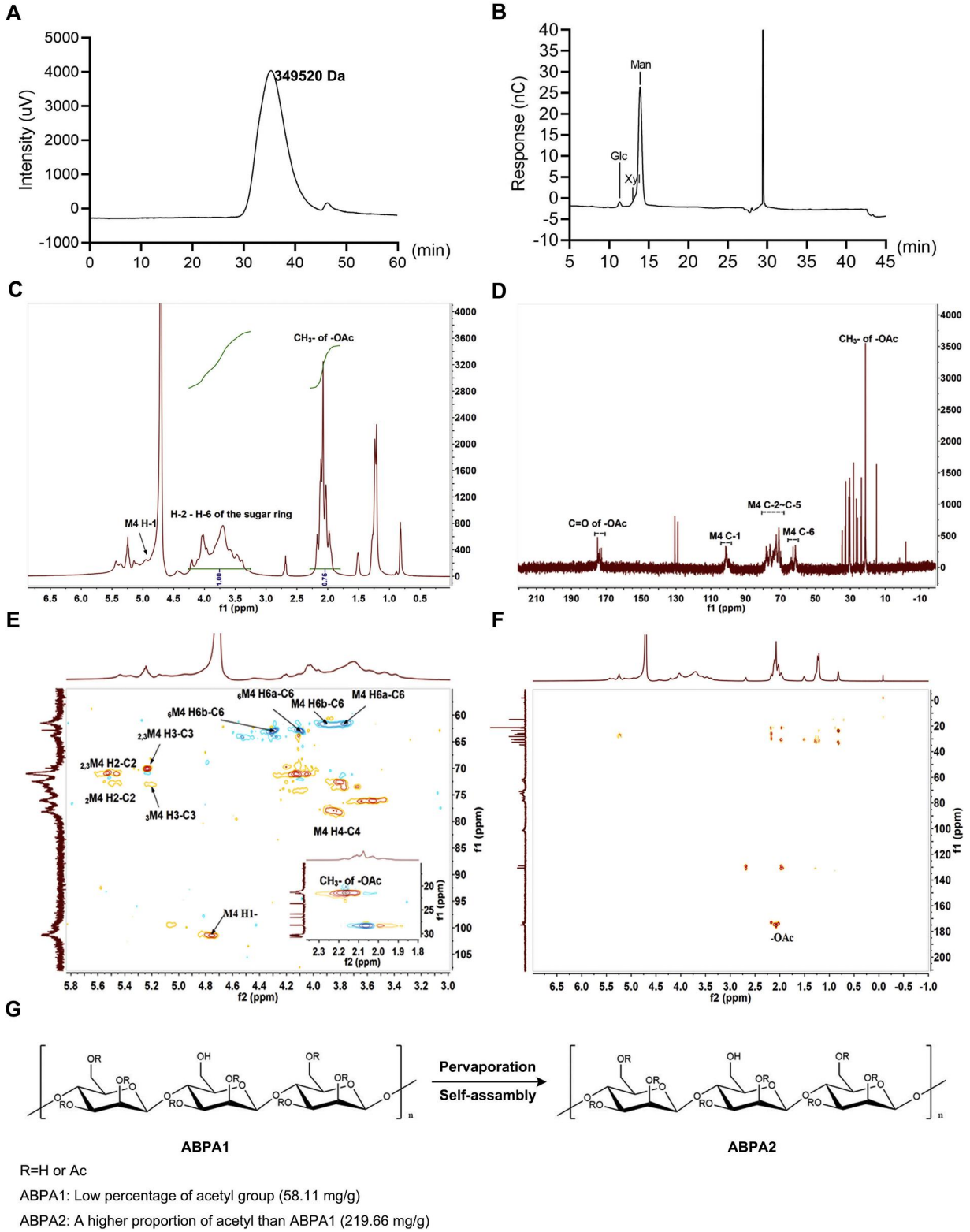

Fig. 2. Structural elucidation of ABPA2. (A) HPGPC evaluated the molecular weight of ABPA2. (B) HPLC chromatogram of monosaccharides composition after acid hydrolysis of ABPA2. (C) ^{1}H NMR spectrum of ABPA2. (D) ^{13}C NMR spectrum of ABPA2. (E) HSQC spectrum of ABPA2. (F) HMBC spectrum of ABPA2. (G) Schematic illustration of the structural transition from ABPA1 to ABPA2. And the O-acetyl content of ABPA1 and ABPA2 in a single assay.

et al., 2022; X et al., 2022). However, its pro-wound healing effect has not been observed. By coincidence, it was found that when ABPA1 was dissolved again in a 20 % aqueous ethanol solution, a polysaccharide membrane formed on the surface during evaporation under normobaric conditions (Fig. 1A).

Over the last few decades, different types of polysaccharides have been used to fabricate membranes (Caridade et al., 2015; Musarurwa & Tavengwa, 2022; Su et al., 2024). Depending on their properties, they have been used as liquid filtration, gas separation, adsorption, pervaporation, and proton exchange membranes (V et al., 2022). We speculated that the formation of polysaccharide membranes may change the physical or chemical properties of ABPA1, which warrants in-depth study. After conditions optimization, the ABPA1 solution can continuously form a polysaccharide film. It is collected every 8 h and repeated up to four times. Take the results of a single test as an example, the solids content of the four successively collected batches of polysaccharide membranes gradually increased from 11 % to 66 %. However, the O-acetyl content decreased from 330.27 mg/g in the first collection to 78.32 mg/g in the last collection (Table S1). We hypothesized that the formation of the O-acetyl group is closely linked to the retention of ethanol molecules in the polysaccharide membrane, but the exact mechanism is unknown. The polysaccharide membrane was purified and obtained a homogeneous polysaccharide described as ABPA2. The microscopic morphology of the two lyophilized polysaccharides (−60 °C, 5 mbar, 24 h) was then compared with a 3D profiler and SEM. SEM imaging accurately depicted the microstructure of ABPA2 and ABPA1. The molecular arrangement and polymerization feature of ABPA2 was in higher order compared to ABPA1, whereas the product (ABPA2) indicated decreased entropy than its reactant (ABPA1). It demonstrated increased enthalpic properties when polymerized into tightly arranged membranes (Fig. 1B-C). The representative image under a 3D profiler also revealed that ABPA2 has a lower roughness than ABPA1 (Fig. 1D-E). Fig. 1D illustrates a representative microscopic area of ABPA1 and indicates that the contour differences for the selected position are 25.2 and 24.0 in the transverse and longitudinal directions, respectively. Correspondingly, the values of ABPA2 are 9.6 and 13.9 (Fig. 1E). This morphological difference implies that the structure of the polysaccharides changes as the pervaporation membrane is produced.

Subsequently, the structure of ABPA2 was systematically characterized using the methods described in previous articles (X et al., 2022). The molecular weight of ABPA2 was 350 kDa, and it was mainly composed of mannose (92.19 %), followed by xylose (4.16 %) and

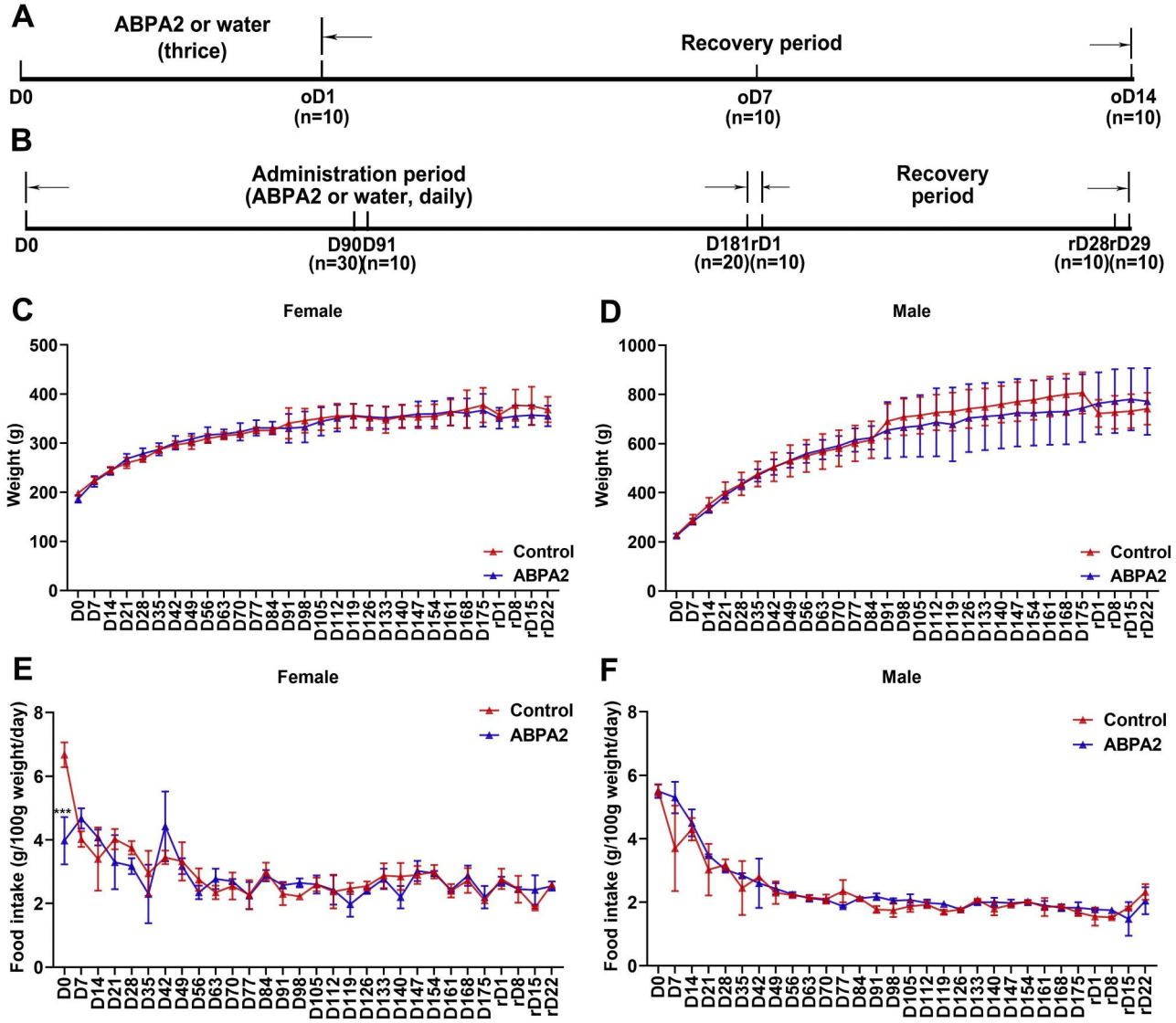

Fig. 3. Body weight and food consumption of SD rats in acute and chronic toxicity studies. (A) Timeline of the acute toxicity study. (B) Timeline of the 180-day chronic toxicity study. Weights of female (C) and male (D) rats in the 180-day chronic toxicity study. Food consumption of female (E) and male (F) rats in the 180-day chronic toxicity study.

glucose (1.81 %) (Figs. 2A-B). The glycosidic linkages of ABPA2, as determined by methylation and GC–MS, are indicated in Table S2. 4-Man(p) accounted for the highest proportion (86.845 %). Based on the comprehensive analysis of the above-mentioned results and NMR spectra, the backbone of ABPA2 is recognized as →4)-β-d-Manp-(1→ which is consistent with ABPA1, but the difference was that ABPA2 has a higher degree of acetyl group substitution at 2-O-, 3-O-, and 6-O- of mannose (Figs. 2C–F). Quantitatively, the O-acetyl content in ABPA1 and ABPA2 was 58.11 and 219.66 mg/kg, respectively (Fig. 2G). However, at present, it is not clear how the acetyl group is introduced into the polysaccharide structure.

The structural analysis explains the film-forming properties of ABPA2 at the microscopic level. On the one hand, the acetyl group is a hydrophobicity group that reduces the hydrophilicity of polysaccharides. On the other hand, introducing acetyl groups increases the number of intra- and intermolecular hydrogen bonds.

3.2. Acute toxicity study of ABPA2

During the 14-day acute toxicity observation period (Fig. 3A), SD rats with ABPA2 treatment did not exhibit abnormal clinical signs or deaths. Body weight was measured at D0, oD1, oD7, and oD14, and there was no statistically significant difference between ABPA2-treated and untreated groups ($p > 0.05$, s Fig. 1). At the end of the acute administration evaluation, pathological examination revealed no lesions or abnormalities in the volume, color, or texture of isolated organs due to ABPA2 treatment.

3.3. 6-month chronic toxicity study of ABPA

Rats with appropriate age and body weight (± 20 % of the mean body weight) were selected for chronic toxicity assessment. Urine and ophthalmological testing were performed during the middle period of administration (D90), the end of administration (D180), and the end of recovery (rD28). The rats were killed in batches the next day (D91, D181, and rD29) for hematological, hematochemical, and pathological examination (Fig. 3B).

Throughout the treatment period, no abnormal clinical symptoms or mortality were evident in all rats in the experimental group. Compared with the control group, there was no statistical difference in body weight between male and female rats in the experimental groups during ABPA2 administration (Fig. 3C-D). The average food intake of the female group (1 g/kg/day) at week one was significantly lower than that of the corresponding control group ($p < 0.05$); however, this observation was not a transient change (Fig. 3E-F). There was no dose or time dependence, and it was not considered relevant to toxicology. Additionally, the control rats and those administered ABPA2 orally appeared to be homogeneously healthy after the four-week recovery period. Therefore, the chronic toxicity test revealed that ABPA2 did not cause death or toxic pathological damage to tissues and organs.

According to the experimental design, SD rats were anesthetized by an intraperitoneal injection of 40 mg/kg pentobarbital sodium solution (30 mg/mL) at the corresponding time points (D91, D181, and rD29) and autopsied immediately after death through abdominal aorta. Pathological gross examination was performed on the skin, body surface, tissues, and organs of the autopsied rats. The body surface of all rats was intact, and their coat was smooth. There was no trauma or ulceration, no subcutaneous hemorrhagic spots and pigmentation, no hydrops in the abdominal and chest cavities, and all organs were in their normal positions. No apparent lesions or abnormalities were observed in the volume, color, and texture of each organ, and the brain coefficient revealed no statistical significance. Critical organ coefficients of male and female rats in each administration group at each stage are shown in Table S3. Individual organ coefficients change only appeared in individual samples. These differences reduced with time after the discontinuation of the drug, and no changes in treatment can be attributed to and or were considered to be of no toxicological significance. Histological analysis demonstrated variations in the livers of animals treated with ABPA2, but no abnormalities were evident in the kidneys, heart, and bone marrow smears (Fig. 4). In the male and female treatment groups, some of the liver samples of SD rats exhibited lobular central hepatocyte hypertrophy (D90), which disappeared at day 29 of rD29, and vacuolar degeneration of hepatocytes recovered similarly to that of the control group (Fig. 4A–F). The above-mentioned changes can be recovered after 28 days of drug withdrawal, which was considered to be caused by the changes in liver adaptability to drugs. There was no significant pathological difference detected between the kidney (Fig. 4G–L), heart (Fig. 4M–R), and bone marrow (Fig. 4S–X) of the animals treated with ABPA2.

Another essential aspect of toxicological evaluation was biochemical parameters. Clinical blood chemistry analysis (Table 1) was performed without significant organic lesions. TBIL in female rats in the ABPA2 treatment group decreased significantly at days D91 and D181 but was on rD29, and other blood biochemical parameters had no significant effect throughout the experimental period ($p > 0.05$). Statistically significant changes observed in this study were within the normal physiological range.

There were no significant differences in GLU, SG, PRO, URO, NIT, or WBC between ABPA2 administered and control groups at different time points ($p > 0.05$). However, significant changes were observed in the following urine indexes (Table S4): BIL and KET of D91 female rats in the ABPA2 treatment group were higher ($p < 0.05$), BLO of D91 male rats in the ABPA2 treatment group was lower ($p < 0.05$), urine pH of D181 female rats in the ABPA2 treatment group was higher ($p < 0.05$), and rD29 male rats in ABPA2 treatment group had more elevated WBC ($p < 0.05$). However, these changes had no apparent time or dose-dependent relationship, and some of the changes were within the background data of the New Southern Drug Evaluation Center; thus, they were considered to have no toxicological significance.

The hematological analysis is an essential indicator of toxicological evaluation, and it compares the hematological parameters of the two experimental groups of rats (Table S5). HGB and HCT levels were significantly lower in the ABPA2 treatment group ($p < 0.05$). After administration, the MCV of female rats ($p < 0.05$) and the EOS of D181 male rats in the ABPA2 treatment group were lower ($p < 0.05$). However, the change occurs without dose-response dependence. The male rats in the ABPA2 treatment group had a shorter PT at D181 days ($p < 0.05$) compared to APTT. In contrast, the APTT coagulation parameters of male rats in the ABPA2 treatment group at each time point were unaffected ($p > 0.05$). At any point, there were no statistically significant differences in other blood indicators between ABPA2 treatment and control groups ($p > 0.05$). Therefore, in SD rats, ABPA2 had no significant effects on hematological parameters, PT, or APTT.

3.4. ABPA2 promotes tail fin regeneration in zebrafish

Many studies have revealed that the polysaccharides in aloe vera are the main component responsible for its beneficial effects on a variety of skin problems(Ad & Ns, 1988; C et al., 2019; Liang et al., 2021c; Zhang et al., 2022). A zebrafish tail fin injury model was used to assess whether ABPA2 can promote caudal fin regeneration. Zebrafish larvae were treated with gradient concentrations to screen the optimal ABPA2 concentration of 0.0375 % (sFigure 2). The effect of ABPA2 on tail fin regeneration in juvenile and adult zebrafish was also investigated (Fig. 5). ABPA2 increased the rate of tail fin regeneration in larval zebrafish (Fig. 5A). At 48, 72, and 120 hpa, the length of caudal fin was significantly longer in the ABPA2-treated group than in the untreated group (Fig. 5B). The daily regeneration rate in the ABPA2 treatment group was significantly greater from 24 hpa to 48 hpa, reaching approximately 1.7 times that of the control group (72.2 mm/day versus 121.8 mm/day) (Fig. 5C). According to the images of caudal fin regeneration, at 48 hpa, the caudal fin of the ABPA2-treated group appeared

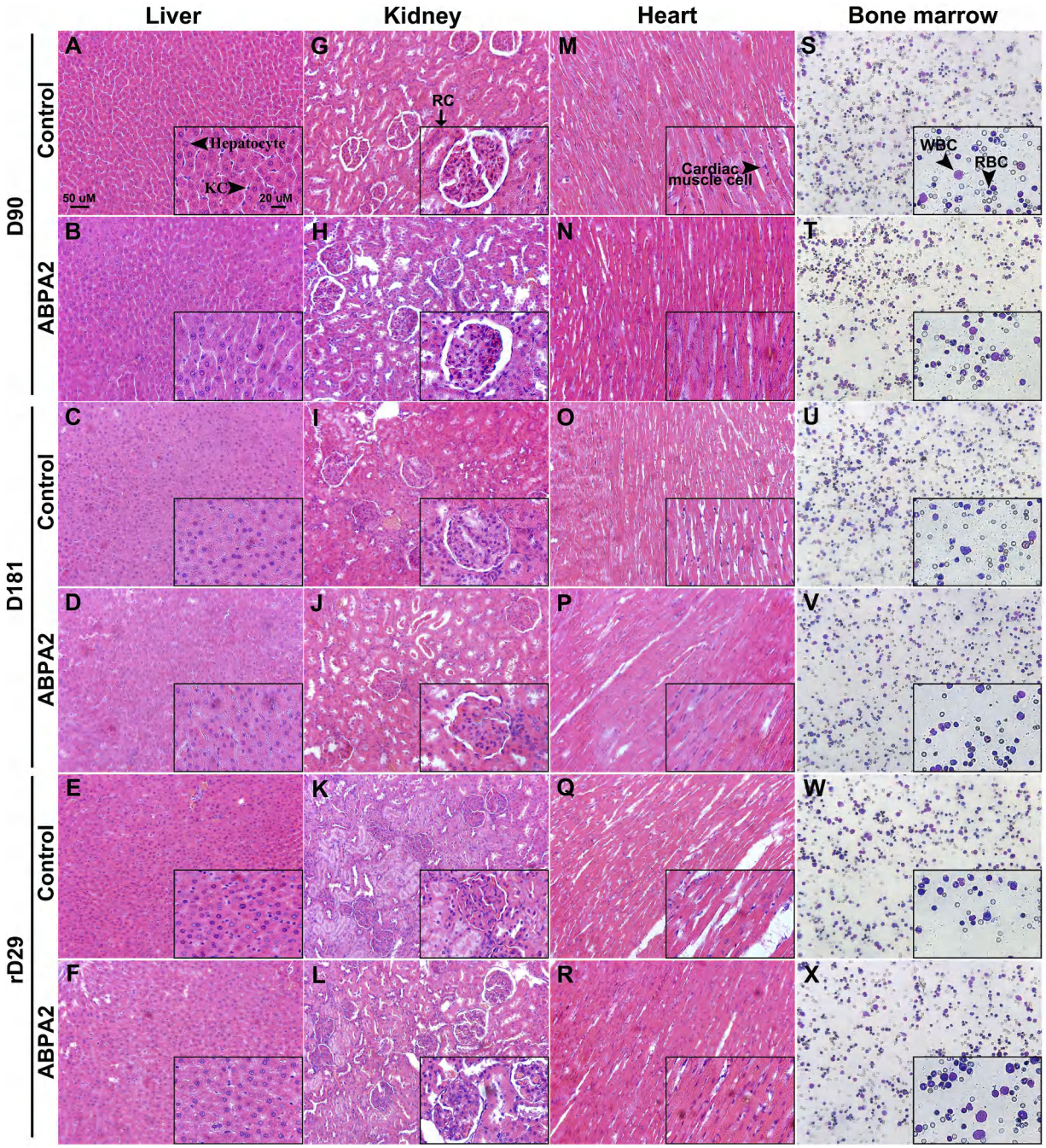

Fig. 4. Histopathological analysis of liver, kidney, and heart in SD rats and bone marrow smears (200 × and 400 ×). (A–F) Liver HE staining. (G–L) Kidney HE staining. (M–R) Heart HE staining. (S–X) Bone marrow smears. The scale bar is illustrated in A. KC, Kupffer cell; RC, renal corpuscle; WBC, white blood cell; RED, red blood cell. Ocular appendages and anterior segments were examined with a direct ophthalmoscope in D90, D180, and rD28, and no ocular abnormalities were observed at different doses. Consequently, it is believed that ABPA2 does not cause toxic damage to the eyes of rats.

better than that of the control group, which remained incomplete at the tip (Fig. 5A, black arrow). To determine whether ABPA2 can accelerate the caudal fin regeneration in adult zebrafish, half of the caudal fin was amputated from 3-month zebrafish, and the fish were treated with or without the compound for 13 days, with the length of the caudal fins measured daily. The data identified that the ABPA2-treated adult zebrafish had a generally higher tail fin regeneration area than the control fish, with the most significant occurring on the 7^{th} day (Fig. 5D-E). These data suggested that ABPA2 can promote the repair and regeneration of tail fins in larval and adult zebrafish.

Based on the above data, it is interesting to know how ABPA2 promotes the regeneration of zebrafish tail fins. First, it was investigated whether ABPA2 can affect cell proliferation in the tail fin wound area during the regeneration process in juvenile fish. After 24 h of tail fin amputation, both groups were treated with 500 μM EdU for 10 h, and the number of EdU-positive cells was counted at the tail fin wound site. The results revealed that between 24 and 34 h post-amputation (Fig. 6A), cell proliferation in the tail fin wound area of the ABPA2 group was significantly increased, with the proliferation rate reaching 2.3 times that of the control group (Fig. 6B). This indicated that drug treatment significantly enhanced cell proliferation at the wound site.

To further investigate the effect of ABPA2 on the expression of inflammation-related genes after tail fin amputation, RT-qPCR was used to assess the expression levels of three pro-inflammatory factors—TNF-

Table 1
Blood biochemistry analysis of SD rats.

Summary of blood biochemical tests (Sex: Female)

Parameter	D91 (n = 5)		D181 (n = 5)		rD29 (n = 5)	
	Control	ABPA2	Control	ABPA2	Control	ABPA2
ALT (U/L)	21.85 ± 6.76	19.8 ± 2.72	62.29 ± 68.17	43.75 ± 10.36	67.21 ± 48.46	45.25 ± 19.54
CRE (μmol/L)	40.16 ± 7.98	33.76 ± 3.26	39.44 ± 1.61	34.66 ± 4.61	39.88 ± 7.82	40.36 ± 5.41
GLU (mmol/L)	6.56 ± 0.66	6.18 ± 0.52	6.66 ± 0.4	6.26 ± 0.83	6.12 ± 0.53	7.11 ± 0.7
Urea (mmol/L)	8.46 ± 1.37	7.87 ± 1.18	6.91 ± 1.2	7.89 ± 0.92	7.63 ± 0.97	8.05 ± 1.82
TBIL (μmol/L)	1.18 ± 0.36	**0.68 ± 0.2***	1.42 ± 0.26	**0.84 ± 0.25***	1.88 ± 0.66	1.66 ± 0.29
ALP (U/L)	40.52 ± 7.63	33.56 ± 7.83	38.36 ± 13.49	29.69 ± 8.7	28.58 ± 5.31	34.41 ± 15
CHOL (mmol/L)	1.61 ± 0.46	2.14 ± 0.41	2.44 ± 0.47	3.13 ± 0.58	2.23 ± 0.44	2.35 ± 0.23
GGT (U/L)	0.15 ± 0.64	0.6 ± 0.22	0.2 ± 0.63	0.61 ± 0.37	0.59 ± 0.26	0.48 ± 0.14
TP (g/L)	60.78 ± 6.85	64.52 ± 1.49	65.47 ± 4.91	69.94 ± 4.27	65.36 ± 2.76	68.8 ± 4.65
ALB (g/L)	42.96 ± 5.82	45.01 ± 0.72	46.6 ± 4.22	49 ± 3.43	43.94 ± 1.85	44.7 ± 3.27
CK (U/L)	423.52 ± 157.59	436.8 ± 215.79	362.23 ± 188.85	240.25 ± 92.38	446.84 ± 104.61	489.28 ± 225.44
TG (mmol/L)	0.99 ± 1.16	0.41 ± 0.03	0.7 ± 0.19	0.71 ± 0.26	0.54 ± 0.18	0.49 ± 0.18
AST (U/L)	88.22 ± 37.42	95.5 ± 15.72	122.58 ± 64.79	101.94 ± 18.78	224.92 ± 129.52	172.86 ± 58.95
Na^+ (mmol/L)	139.6 ± 1.12	141.86 ± 0.66	143.74 ± 1.2	144.38 ± 0.68	143.36 ± 0.78	143.68 ± 1.79
K^+ (mmol/L)	4.33 ± 0.24	4.43 ± 0.28	4.4 ± 0.47	4.05 ± 0.18	4.03 ± 0.21	4.13 ± 0.18
Cl^- (mmol/L)	107.82 ± 0.72	108.22 ± 0.86	106.86 ±2	105.92 ±0.86	107.7 ± 0.44	107.12 ± 1.49

Summary of blood biochemical tests (Sex: Male).

Parameter	D91 (n = 5)		D181 (n = 5)		rD29 (n = 5)	
	Control	ABPA2	Control	ABPA2	Control	ABPA2
ALT (U/L)	26.02 ± 6.98	24.46 ± 3.51	33.49 ± 4.07	32.06 ± 5.42	67.21 ± 48.46	45.25 ± 19.54
CRE (μmol/L)	34.76 ± 8.99	33.92 ± 6.11	29.66 ± 3.71	32.02 ± 6.15	39.88 ± 7.82	40.36 ± 5.41
GLU (mmol/L)	6.88 ± 0.95	6.73 ± 0.78	7.89 ± 1.43	7.16 ± 0.91	6.12 ± 0.53	7.11 ± 0.7
Urea (mmol/L)	6.92 ± 1.71	6.24 ± 0.86	6.03 ± 1.05	5.99 ± 0.85	7.63 ± 0.97	8.05 ± 1.82
TBIL (μmol/L)	1.14 ± 0.23	0.98 ± 0.33	1.52 ± 0.23	1.3 ± 0.32	1.88 ± 0.66	1.66 ± 0.29
ALP (U/L)	87.34 ± 13.78	78.97 ± 16.58	70.52 ± 9.74	75.31 ± 16.26	28.58 ± 5.31	34.41 ± 15
CHOL (mmol/L)	1.53 ± 0.24	1.57 ± 0.2	1.68 ± 0.25	1.88 ± 0.16	2.23 ± 0.44	2.35 ± 0.23
GGT (U/L)	0.47 ± 0.44	0.46 ± 0.24	0.33 ± 0.29	0.59 ± 0.25	0.59 ± 0.26	0.48 ± 0.14
TP (g/L)	55.12 ± 2.8	56.74 ± 2.75	59.54 ± 3.04	57.07 ± 3.04	65.36 ± 2.76	68.8 ± 4.65

Table 1 (*continued*)

Summary of blood biochemical tests (Sex: Male).

Parameter	D91 (n = 5)		D181 (n = 5)		rD29 (n = 5)	
	Control	ABPA2	Control	ABPA2	Control	ABPA2
ALB (g/L)	38.39 ± 2.17	39.21 ± 2.03	41.15 ± 1.73	40.25 ± 0.95	43.94 ± 1.85	44.7 ± 3.27
CK (U/L)	504.2 ± 119.49	542.47 ± 150.05	407.89 ± 116.84	563.94 ± 274	446.84 ± 104.61	489.28 ± 225.44
TG (mmol/L)	0.41 ± 0.1	0.42 ± 0.14	0.91 ± 0.24	0.8 ± 0.52	0.54 ± 0.18	0.49 ± 0.18
AST (U/L)	115.74 ± 20.49	117.02 ± 10.81	109.24 ± 18.52	125.18 ± 15.39	224.92 ± 129.52	172.86 ± 58.95
Na+ (mmol/L)	139.76 ± 1.91	142.94 ± 1.39	144.2 ± 1.09	144.2 ± 0.75	143.36 ± 0.78	143.68 ± 1.79
K+ (mmol/L)	4.55 ± 0.14	4.37 ± 0.17	4.41 ± 0.26	4.5 ± 0.26	4.03 ± 0.21	4.13 ± 0.18
Cl- (mmol/L)	106.22 ± 1.66	106.5 ± 1.6	104.12 ± 1.54	105.24 ± 1.38	107.7 ± 0.44	107.12 ± 1.49

* Represent the significance level for the difference with the control group for $p < 0.05$.

α, IL-1, and IL-8 at 0, 3, 6, 12, and 24 h post-amputation. Notably, within 3 h of amputation, TNF-α, IL-1β, and IL-8 were higher in the ABPA2 treatment group than the control group. However, from 3 to 24 h, the expression of TNF-α, IL-1, and IL-8 in the ABPA2 treatment group gradually decreased (Fig. 6C–E). These results indicated that ABPA2 enhances the expression of pro-inflammatory genes such as TNF-α, IL-1, and IL-8 during the initial phase of caudal fin regeneration, specifically the inflammatory stage. In the later stages of inflammation and repair, macrophages play a crucial role in fin regeneration by phagocytosing cell debris and bacteria, producing anti-inflammatory cytokines, and regulating the inflammatory response. These results suggest that the level of pro-inflammatory factors reached a rapid peak and then fall back to basal levels. The wound then enters a phase of rapid proliferation and regeneration.

3.5. *Effect of ABPA2 on the inflammatory response after the caudal fin amputation*

Neutrophils are an essential class of innate immune cells (Peña & Martin, 2024; Reinke & Sorg, 2012; Summers et al., 2010). They are the first phagocytes to be recruited to sterile inflammation sites, and they facilitate the removal of dead or damaged cells and harmful substances (Silvestre-Roig et al., 2019). To explore whether ABPA2 had an effect on neutrophil migration after caudal fin amputation, the number of neutrophils at the wound site was counted using the transgenic zebrafish Tg (lyz: DsRed2), specifically labeling neutrophils. The results revealed no significant difference between the number of neutrophils at the wound site of the ABPA2-treated group and the control group at each time point from 0 to 8 h after caudal fin cutting, indicating that ABPA2 has no apparent effect on the migration of neutrophils to the wound (Fig. 6F-G).

The macrophages play a central role in the inflammatory and repair phases of fin regeneration by phagocytosing cell debris and bacteria, producing inflammatory cytokines, and regulating the inflammatory response (Sharifiaghdam et al., 2022). To investigate if ABPA2 affected macrophages at the wound site, they were counted using the transgenic line Tg2 (mpeg: EGFP), specifically labeling macrophages (Fig. 6H).

It was revealed that the macrophages at the wound site in the ABPA2 treatment group exhibited a rapid increase in the first 12 h (Fig. 6I). Maintaining a relatively high level of macrophages during the pre-inflammatory phase allows the wound to quickly progress through the inflammatory phase, accelerating tissue repair. At 96 hpa, the number of

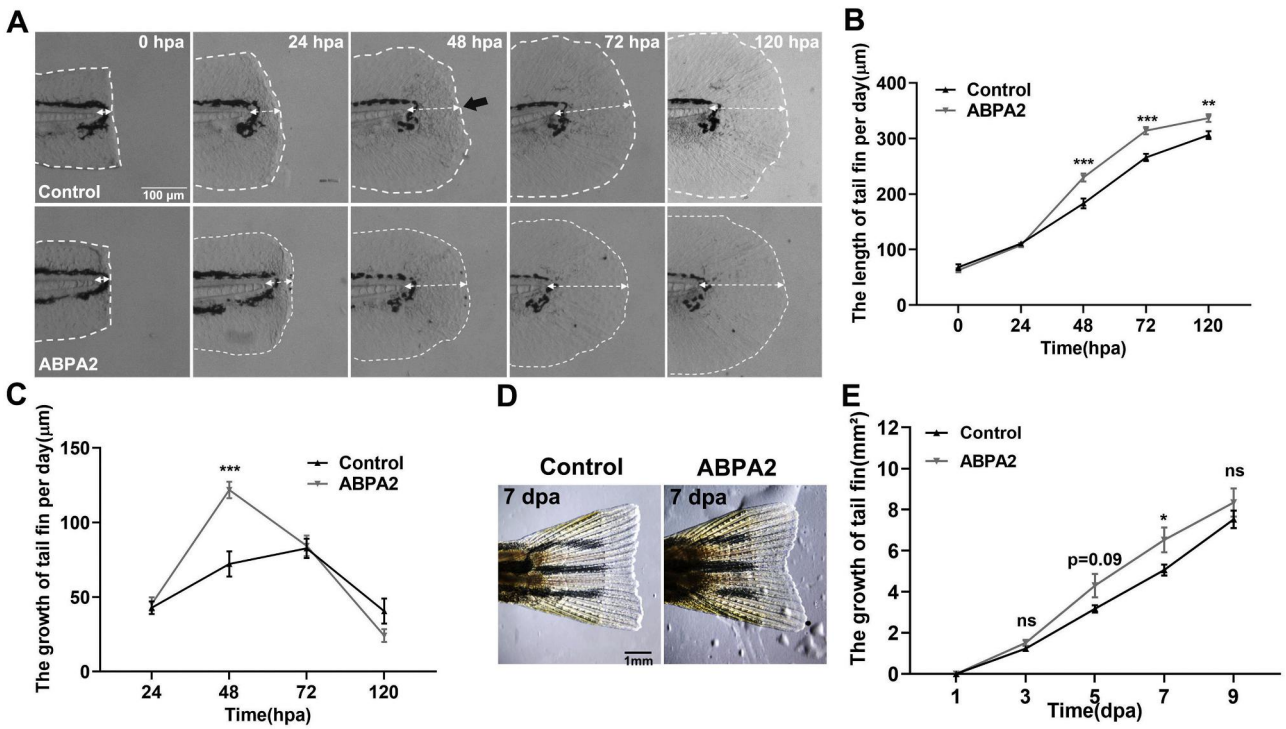

Fig. 5. ABPA2 promotes tail fin regeneration. (A) Representative images revealing caudal fin length of zebrafish larvae with or without exposure to ABPA2 from 0 hpa to 120 hpa. (B) The caudal fin length measured at different time. (C) The length of growth in zebrafish tail fins every 24 h. (D) Representative images exhibiting zebrafish (adult) tail fin with or without exposure to ABPA2 for 7 dpa. (E) The length of the tail fin according to statistical analysis. Statistical analysis was performed using a two-tailed unpaired *t*-test. The asterisks indicate a statistically significant difference (*$p < 0.05$, **$p < 0.01$, ***$p < 0.001$).

macrophages in the ABPA2 treatment group was significantly lower than in the control group, and it was close to the initial number (Fig. 6I). These results concluded that ABPA2 can greatly accelerate the regeneration and repair process of zebrafish tail fins. By 96 hpa, the ABPA2 treatment group had essentially completed tail fin repair, while the tail fin regeneration of the control group tail was still ongoing and still required macrophages.

3.6. Potential molecular mechanisms of ABPA2 in promoting caudal fin regeneration

To investigate the molecular mechanism of ABPA2 in promoting caudal fin regeneration, bulk RNA-seq was performed using the ABPA2-treated embryos at two-time points; one was 6 hpa during the inflammatory phase, whereas the other was 36 hpa during the repair phase (Fig. 7, sFigure3). The gene-concept network revealed many genes coding collagen, laminin, integrin, and myosin were enriched in signaling pathways for extracellular matrix and skeletal reconstruction, such as extracellular matrix structural constituent, glycosaminoglycan binding, protein-contain complex binding, actin filament binding, structural constituent of muscle. (Fig. 7A, sFigure 3E). GO analysis of molecular functions also revealed that the up-regulated genes were predominantly enriched in the categories relative to cell adhesion and extracellular matrix organization. Besides, genes related to the development of multiple organs were upregulated (Fig. 7B).

The extracellular matrix provides mechanical signals that ensure smooth cells communication with each other and with their environment. GO analysis also showed an upregulation of the calcium ion transporter in Fig. 7B. As the second messenger, calcium plays a crucial role in the process of cell differentiation, mitochondria function and ECM. Here, all calcium transporters showed an upward trend, and four of them were significantly upregulated (Fig. 7C).

Mitochondrial dynamics play a central role in drug-promoted zebrafish tail fin regeneration by regulating changes in mitochondrial morphology and function, which affects the metabolic state and biological behavior of cells, thereby promoting tissue regeneration(F et al., 2024). During the regeneration process of the zebrafish tail fin, the dynamic changes of mitochondria involve processes such as mitochondrial biosynthesis, fission, fusion, transport, and autophagy, all regulated by numerous proteins and enzymatic reactions. For instance, mitochondrial fusion proteins (Mfn1/2 and Opa1), autophagy proteins (Pink1 and Sqstm1), and nuclear-encoded genes related to mitochondrial biosynthesis (Ppargc1a and TFAM) are all important genes associated with mitochondrial dynamics(Aw et al., 2018). The expression of mitochondrial dynamics-related genes was detected using RT-qPCR, and the results revealed that the expression of these genes in 0.625 % and 1.5625 % ABPA2 treatment groups was significantly higher than that in the control group (Fig. 7D). Overall, these genes and mitochondrial dynamics are involved in maintaining mitochondrial morphology, cell adhesion, and extracellular matrix adhesion, collectively promoting the regeneration of the zebrafish tail fin. In summary, ABPA2 promotes zebrafish tail fin regeneration by affecting the cytokine network and mitochondrial dynamics, and these findings provide potential targets and mechanisms for developing new regenerative-promoting drugs.

4. Discussion

Acetylated mannan has been identified to have various biological activities (Bai et al., 2023; C et al., 2019). One study revealed that acemannan obtained from aloe vera induced cell proliferation, as well as VEGF and collagen I expression. However, this biological activity disappeared after 100 % deacetylation (J et al., 2015). Acetyl groups are critical for the biological functions of mannan, as evidenced by many studies (J et al., 2015; Kumar & Kumar 2019; Salah et al., 2017). Similarly, the regenerative effect of ABPA2 was observed, which ABPA1 does not exhibit. In order to further previous finding, the zebrafish fin wounding model was involved to investigate functional significance of acemannan.

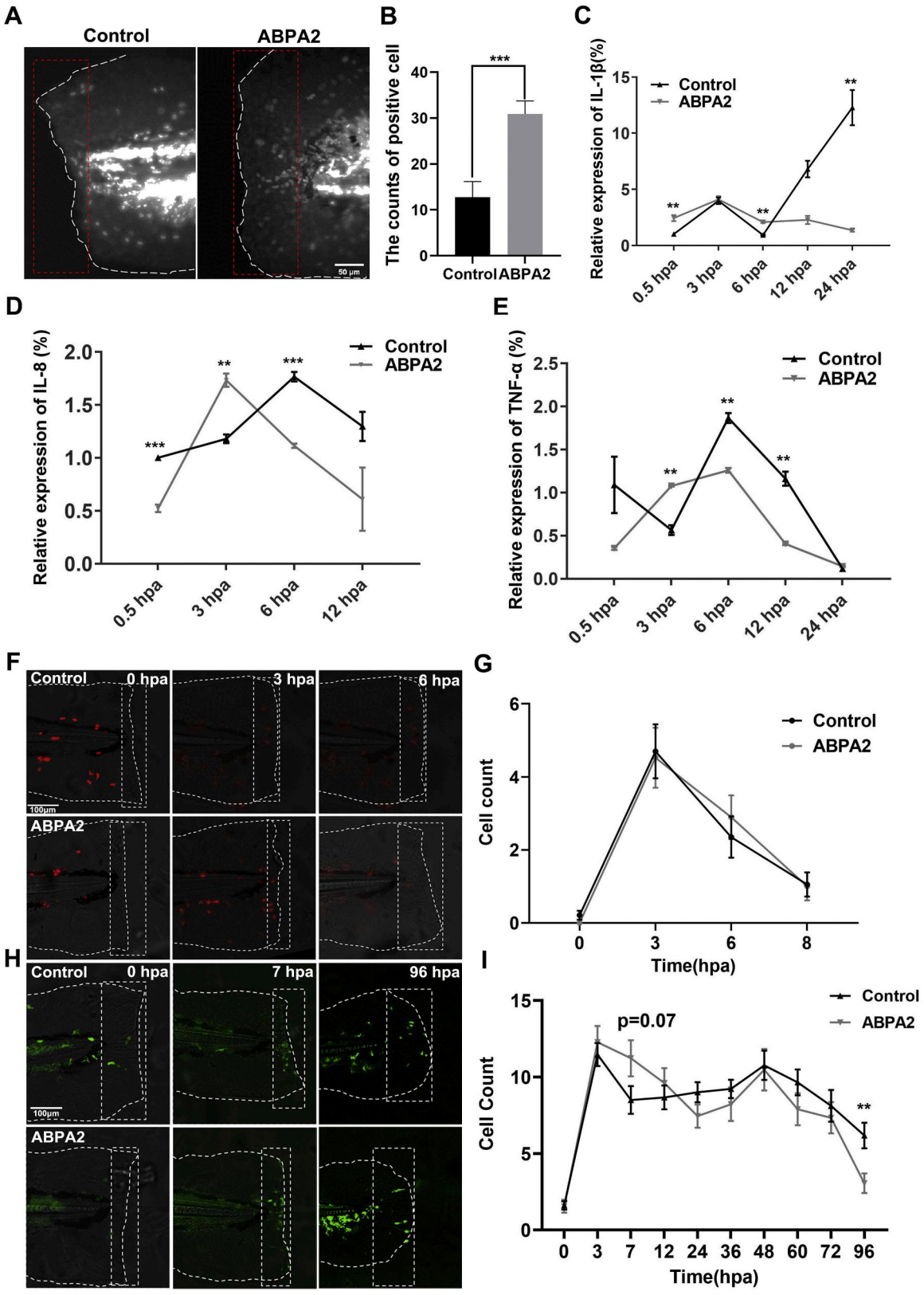

Fig. 6. Cell proliferation and anti-inflammatory effects of ABPA2. (A) Representative images revealing EdU-positive cells at the tail fin wound site of zebrafish larvae. (B) EdU-positive cells counts in the wound. (C–E) Expression of inflammation-related genes with or without exposure to ABPA2 from 0 hpa to 24 hpa. (F) Tg (lyz: DsRed2) transgenic zebrafish were used to examine the dynamic changes in neutrophil migration. (G) Variation in the number of neutrophils in zebrafish tail with exposure time in ABPA2. (H) Tg2 (mpeg1: EGFP) transgenic zebrafish were used to examine the dynamic changes in macrophage migration. (I) Variation in the number of macrophages in zebrafish tail with exposure time in ABPA2. Statistical analysis was performed using a two-tailed unpaired t-test. The asterisks indicate a statistically significant difference (*$p < 0.05$, **$p < 0.01$, ***$p < 0.001$).

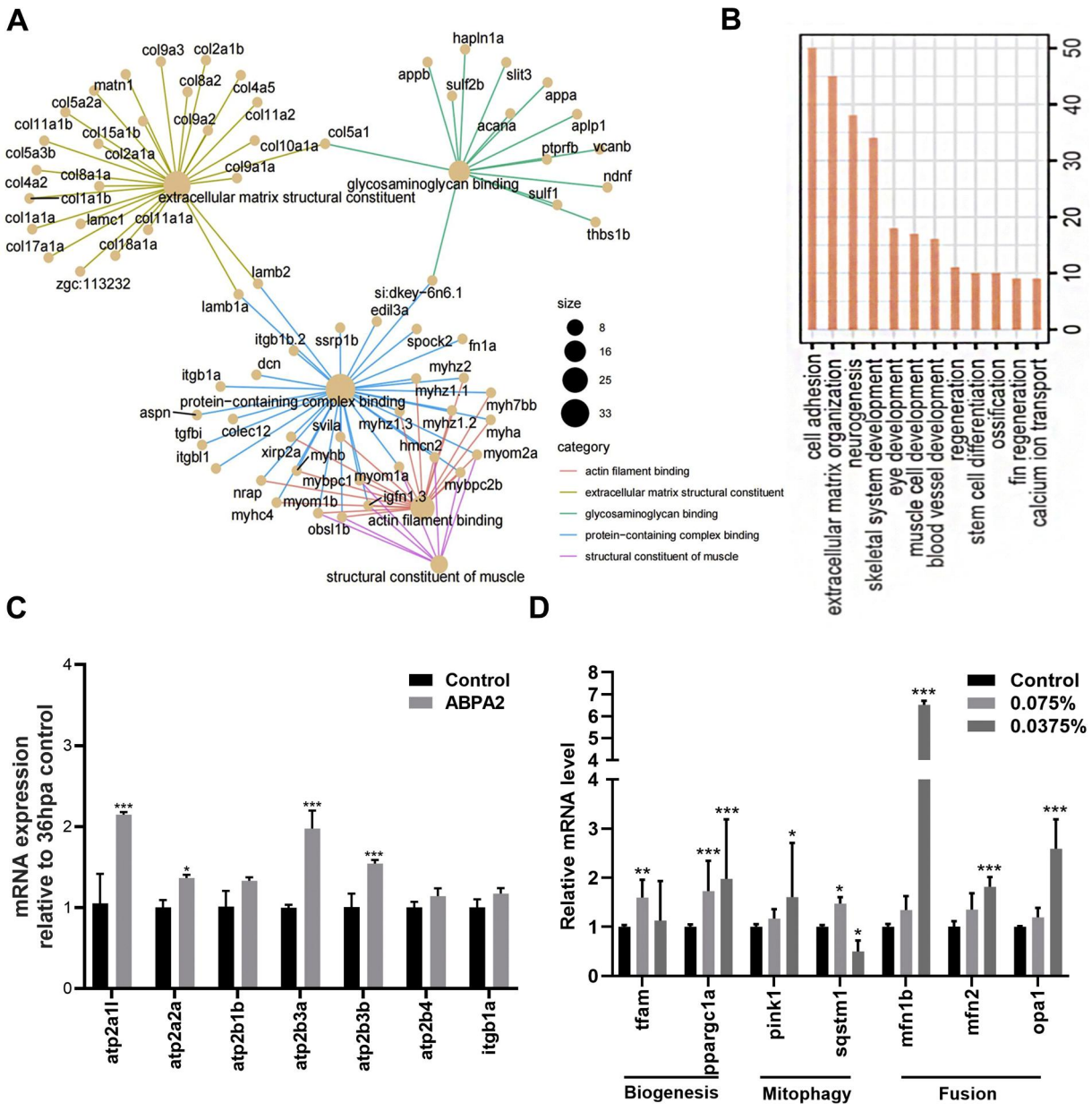

Fig. 7. ABPA2 affects key metabolic processes. (A) Gene-concept network. (B) Zebrafish (72 hpf) were analyzed by bulk RNA-seq after ABPA2 treatment for 36 h. GO clustering analysis was performed on the up-regulated expression genes. (C) RT-qPCR analysis was used to assess gene expression associated with calcium ion transport genes. (D) RT-qPCR analysis was used to assess gene expression associated with mitochondrial dynamics. Statistical analysis was performed using the two-tailed unpaired t-test. The asterisks indicate a statistically significant difference (*$p < 0.05$, **$p < 0.01$, ***$p < 0.001$).

The degree of acetylation affects the solubility, bio-accessibility, and even biological activity of polysaccharides (Wang et al., 2024). Researchers have devised various methods to enhance the degree of acetylation in polysaccharides, such as aqueous media, microwave-assisted acetylation, ultrasound-assisted acetylation, and enzyme-catalyzed acetylation (Li et al., 2023; Liu et al., 2023). This study is the first to reveal that highly acetylated mannan can be obtained by polysaccharide self-assembly using the membrane-forming properties of polysaccharides (Fig. 2G). This approach minimizes the use of toxic solvents, enhancing its biocompatibility and safety. Furthermore, the chemical modification process frequently reduces the molecular weight of polysaccharides (Liu et al., 2023). However, the results of this study identified that there is little difference in the molecular weights of ABPA1 and ABPA2. Additionally, the difference in the microstructure of the two polysaccharides (Fig. 1) suggests that the acetyl group greatly increases the intermolecular force of the polysaccharide, implying that the molecule contains higher energy. This allowed the polysaccharide to form a interactable surface facilitating cell-membrane interaction. And more importantly, the water dissolubility of this polysaccharide was significantly increased. It is able to be readily dissolved in aqueous culturing medium of zebrafish. Moreover, it did exert wound healing effects after dissolving in water. All these hinted at acetyl functional group played important role in terms of dissolubility and dispersal ability of acemannan polysaccharide.

After all, high dissolubility plausibly permits the biological activity of acemannan polysaccharide. Wound healing therefore was promoted by aqueous distribution of the polysaccharide. This phenomenon recapitulates that wound healing is tightly regulated by anti-inflammatory macrophage. Macrophages effectively extravasated to obtain optimal wound healing. Insomuch as macrophage plays a critical role in coordinating and regulating dynamic process of wound healing. Moreover, metabolic regulation is the key of effectively integrating the dynamic

process of wound healing (Eming et al., 2021; Niu et al., 2017). It therefore, mitochondrial biogenesis was significantly increased as well as mitochondrial fusion and fission. It indicated that mitochondrial metabolism was actively regulated by culturing with the polysaccharide. At the same time, genes of calcium transportation were upregulated. It feasible regulated mechanotransduction to promote metabolic regulation. And in RNA-seq, genes of extracellular matrix were increased. All together with electron microscopic assay, it strongly supported that the dissoluble polysaccharide in all likelihood exerted its macrophage regulation through interaction with wounding surface. It was in line with regular experience in applying aloe gel to wounding skin. The interaction was able to enhance cell adhesion to allow extravasation of macrophage. In this research, macrophage was defined as a de novo target of immuno-regulator of aloe polysaccharide. And acetylation of mannana could increase the dissolubility and membrane formation ability to facilitate biological function of polysaccharide. At last, it suggested an extracellular matrix regulatory mechanism of polysaccharide to promote effective wound healing. However, it is noteworthy that zebrafish have a strong regenerative capacity, allowing them to regenerate a wide range of tissues and organs, including fins, hearts, spinal cords, and so on (Marques et al., 2019). Though it is a promising phenomenon, it may still be ineffective in the mammalian wound healing process. It therefore warrants further research in mammalian wound healing.

5. Conclusion

We obtained a highly acetylated mannan (ABPA2) by exploiting of the self-assembly properties of the evaporated aloe vera polysaccharide membrane. The safety of ABPA2 was established through systemic acute and chronic toxicity studies conducted in Sprague-Dawley (SD) rats. Subsequent functional investigations demonstrated that ABPA2 significantly enhanced tail fin regeneration in both juvenile and adult zebrafish. The effects were in all likelihood ascribed to its ability to induce proliferation and macrophage extravasation in wounded tail fin. By applying RAN seq, it showed that ABPA2 triggered multiple types of cells differentiated and proliferation mainly through regulating genes expression of extracellular matrix.

CRediT authorship contribution statement

Di Li: Writing – original draft, Visualization, Validation, Methodology. **Jiajie Deng:** Visualization, Validation, Formal analysis. **Mengmeng Wang:** Writing – original draft, Visualization, Data curation. **Haiyang Yin:** Visualization, Validation, Resources. **Jinzi Chen:** Writing – review & editing, Writing – original draft, Visualization, Data curation. **Weijie Xu:** Visualization, Validation. **Xiaofeng Guo:** Project administration, Funding acquisition, Formal analysis, Data curation. **Xueli Tong:** Writing – review & editing, Writing – original draft, Visualization, Validation, Data curation. **Ding Ye:** Writing – review & editing, Supervision, Funding acquisition, Formal analysis. **Jiejing Li:** Writing – review & editing, Validation, Supervision, Project administration, Investigation, Funding acquisition, Formal analysis.

Declaration of competing interest

The authors declare that they have no known competing financial interests or personal relationships that could have appeared to influence the work reported in this paper

Acknowledgments

This research was supported by the National Key R&D Program of China (No: 2023YFF0724602), the National Natural Science Foundation of China (No: 82203526), the Guangdong Basic and Applied Basic Research Foundation (No: 2020A1515111135), Young Talent Support Project of Guangzhou Association for Science and Technology (No: QT2024–036), Guangdong Provincial Key Laboratory of Drug Non-Clinical Evaluation and Research (2023B1212070029).

Supplementary materials

Supplementary material associated with this article can be found, in the online version, at doi:10.1016/j.carpta.2025.100709.

Data availability

Data will be made available on request.

References

Ad, K., & Ns, P. (1988). Aloe vera. *Journal of The American Academy of Dermatology, 18*(4). https://doi.org/10.1016/s0190-9622(88)70095-x. Pt 1.

Aw, E.-H., J, S., M, A., & F, S. (2018). Mitochondrial dynamics: Biological roles, molecular machinery, and related diseases. *Molecular Genetics and Metabolism, 125*(4). https://doi.org/10.1016/j.ymgme.2018.10.003

Bai, Y., Niu, Y., Qin, S., & Ma, G. (2023). A new biomaterial derived from aloe vera—Acemannan from basic studies to clinical application. *Pharmaceutics, 15*(7), 1913. https://doi.org/10.3390/pharmaceutics15071913

Bustin, S. A., Benes, V., Garson, J. A., Hellemans, J., Huggett, J., Kubista, M., Mueller, R., Nolan, T., Pfaffl, M. W., Shipley, G. L., Vandesompele, J., & Wittwer, C. T. (2009). The MIQE guidelines: Minimum information for publication of quantitative real-time PCR experiments. *Clinical Chemistry, 55*(4), 611–622. https://doi.org/10.1373/clinchem.2008.112797

C, L., Y, C., F, P., Y, C., Y, G., & H, Q (2019). Extraction, purification, structural characteristics, biological activities and pharmacological applications of acemannan, a polysaccharide from aloe vera: A review. *Molecules (Basel, Switzerland), 24*(8). https://doi.org/10.3390/molecules24081554

Caridade, S. G., Monge, C., Almodóvar, J., Guillot, R., Lavaud, J., Josserand, V., Coll, J.-L., Mano, J. F., & Picart, C. (2015). Myoconductive and osteoinductive free-standing polysaccharide membranes. *Acta Biomaterialia, 15*, 139–149. https://doi.org/10.1016/j.actbio.2014.12.027

Catalano, A., Ceramella, J., Iacopetta, D., Marra, M., Conforti, F., Lupi, F. R., Gabriele, D., Borges, F., & Sinicropi, M. S. (2024). Aloe vera-an extensive review focused on recent studies. *Foods (Basel, Switzerland), 13*(13), 2155. https://doi.org/10.3390/foods13132155

Chelu, M., Musuc, A. M., Popa, M., & Calderon Moreno, J. (2023). Aloe vera-based hydrogels for wound healing: Properties and therapeutic effects. *Gels (Basel, Switzerland), 9*(7), 539. https://doi.org/10.3390/gels9070539

Cock, I. E. (2015). The genus aloe: Phytochemistry and therapeutic uses including treatments for gastrointestinal conditions and chronic inflammation. *Progress in Drug Research. Fortschritte Der Arzneimittelforschung. Progres Des Recherches Pharmaceutiques, 70*, 179–235. https://doi.org/10.1007/978-3-0348-0927-6_6

Eming, S. A., Murray, P. J., & Pearce, E. J. (2021). Metabolic orchestration of the wound healing response. *Cell Metabolism, 33*(9), 1726–1743. https://doi.org/10.1016/j.cmet.2021.07.017

F, C., S, P., L, T., H, Z., H, Z., Y, Y., X, H., Q, W., X, C., Sh, C., & S, X. (2024). Radix rehmanniae praeparata promoted zebrafish fin regeneration through aryl hydrocarbon receptor-dependent autophagy. *Journal of Ethnopharmacology, 331*. https://doi.org/10.1016/j.jep.2024.118272

Hamman, J. H. (2008). Composition and applications of aloe vera leaf gel. *Molecules (Basel, Switzerland), 13*(8), 1599–1616. https://doi.org/10.3390/molecules13081599

Hekmatpou, D., Mehrabi, F., Rahzani, K., & Aminiyan, A. (2019). The effect of aloe vera clinical trials on prevention and healing of skin wound: A systematic review. *Iranian Journal of Medical Sciences, 44*(1), 1–9.

Huang, Y.-N., Chen, K.-C., Wang, J.-H., & Lin, Y.-K. (2024). Effects of aloe vera on burn injuries: A systematic review and meta-analysis of randomized controlled trials. *Journal of Burn Care & Research: Official Publication of the American Burn Association, 45*(6), 1536–1545. https://doi.org/10.1093/jbcr/irae061

J, C., W, T., P, S., V, R., S, J., & P, T (2015). Deacetylation affects the physical properties and bioactivity of acemannan, an extracted polysaccharide from aloe vera. *Carbohydrate Polymers, 133*. https://doi.org/10.1016/j.carbpol.2015.07.039

K, E., & Q, H (2004). Aloe vera: A valuable ingredient for the food, pharmaceutical and cosmetic industries–a review. *Critical Reviews in Food Science and Nutrition, 44*(2). https://doi.org/10.1080/10408690490424694

Kloter, E., Albanese, F., Schweighoffer, R., & Wolf, U. (2023). Phytotherapy in paediatric skin disorders—A systematic literature review. *Complementary Therapies in Medicine, 74*, 102942. https://doi.org/10.1016/j.ctim.2023.102942

Kumar, R., Singh, A. K., Gupta, A., Bishayee, A., & Pandey, A. K. (2019). Therapeutic potential of aloe vera-a miracle gift of nature. *Phytomedicine: International Journal of Phytotherapy and Phytopharmacology, 60*, Article 152996. https://doi.org/10.1016/j.phymed.2019.152996

Kumar, S., & Kumar, R. (2019). Role of acemannan O-acetyl group in murine radioprotection. *Carbohydrate Polymers, 207*, 460–470. https://doi.org/10.1016/j.carbpol.2018.12.003

Li, H., Wang, Y., Zhao, P., Guo, L., Huang, L., Li, X., & Gao, W. (2023). Naturally and chemically acetylated polysaccharides: Structural characteristics, synthesis,

activities, and applications in the delivery system: A review. *Carbohydrate Polymers, 313*, Article 120746. https://doi.org/10.1016/j.carbpol.2023.120746

Li, L., Xu, W., Luo, Y., Lao, C., Tong, X., Du, J., Huang, B., Li, D., Chen, J., Ye, H., Cong, F., Guo, X., & Li, J. (2022). Aloe polymeric acemannan inhibits the cytokine storm in mouse pneumonia models by modulating macrophage metabolism. *Carbohydrate Polymers, 297*, Article 120032. https://doi.org/10.1016/j.carbpol.2022.120032

Liang, J., Cui, L., Li, J., Guan, S., Zhang, K., & Li, J. (2021a). Aloe vera: A medicinal plant used in skin wound healing. *Tissue Engineering. Part B, Reviews, 27*(5), 455–474. https://doi.org/10.1089/ten.TEB.2020.0236

Liang, J., Cui, L., Li, J., Guan, S., Zhang, K., & Li, J. (2021b). Aloe vera: A medicinal plant used in skin wound healing. *Tissue Engineering. Part B, Reviews, 27*(5), 455–474. https://doi.org/10.1089/ten.TEB.2020.0236

Liang, J., Cui, L., Li, J., Guan, S., Zhang, K., & Li, J. (2021c). Aloe vera: A medicinal plant used in skin wound healing. *Tissue Engineering. Part B, Reviews, 27*(5), 455–474. https://doi.org/10.1089/ten.TEB.2020.0236

Liu, C., Cui, Y., Pi, F., Cheng, Y., Guo, Y., & Qian, H. (2019). Extraction, purification, structural characteristics, biological activities and pharmacological applications of acemannan, a polysaccharide from aloe vera: A review. *Molecules (Basel, Switzerland), 24*(8), 1554. https://doi.org/10.3390/molecules24081554

Liu, T., Ren, Q., Wang, S., Gao, J., Shen, C., Zhang, S., Wang, Y., & Guan, F. (2023). Chemical modification of polysaccharides: A review of synthetic approaches, biological activity and the structure–activity relationship. *Molecules, 28*(16), 16. https://doi.org/10.3390/molecules28166073

Marques, I. J., Lupi, E., & Mercader, N. (2019). Model systems for regeneration: Zebrafish. *Development (Cambridge, England), 146*(18), Article dev167692. https://doi.org/10.1242/dev.167692

Minjares-Fuentes, R., Femenia, A., Comas-Serra, F., & Rodríguez-González, V. M. (2018). Compositional and structural features of the main bioactive polysaccharides present in the aloe vera plant. *Journal of AOAC International, 101*(6), 1711–1719. https://doi.org/10.5740/jaoacint.18-0119

Mr, T., A, O., & A, M. (2014). Polysaccharides of aloe vera induce MMP-3 and TIMP-2 gene expression during the skin wound repair of rat. *International Journal of Biological Macromolecules, 65*. https://doi.org/10.1016/j.ijbiomac.2014.01.055

Musarurwa, H., & Tavengwa, N. T. (2022). Application of polysaccharide-based metal organic framework membranes in separation science. *Carbohydrate Polymers, 275*, Article 118743. https://doi.org/10.1016/j.carbpol.2021.118743

Niu, Y., Li, Q., Xie, R., Liu, S., Wang, R., Xing, P., Shi, Y., Wang, Y., Dong, L., & Wang, C. (2017). Modulating the phenotype of host macrophages to enhance osteogenesis in MSC-laden hydrogels: Design of a glucomannan coating material. *Biomaterials, 139*, 39–55. https://doi.org/10.1016/j.biomaterials.2017.05.042

Peña, O. A., & Martin, P. (2024). Cellular and molecular mechanisms of skin wound healing. *Nature Reviews. Molecular Cell Biology, 25*(8), 599–616. https://doi.org/10.1038/s41580-024-00715-1

Reinke, J. M., & Sorg, H. (2012). Wound repair and regeneration. *European Surgical Research. Europaische Chirurgische Forschung. Recherches Chirurgicales Europeennes, 49*(1), 35–43. https://doi.org/10.1159/000339613

Sahebnasagh, A., Saghafi, F., Ghasemi, A., Akbari, J., Alipour, A., Habtemariam, S., Safdari, M., Ghaleno, H. R., & Salehifar, E. (2022). Aloe vera for prevention of acute radiation proctitis in colorectal cancer a preliminary randomized, placebo-controlled clinical trial. *Journal of Gastrointestinal Cancer, 53*(2), 318–325. https://doi.org/10.1007/s12029-021-00597-y

Salah, F., Ghoul, Y. E., Mahdhi, A., Majdoub, H., Jarroux, N., & Sakli, F. (2017). Effect of the deacetylation degree on the antibacterial and antibiofilm activity of acemannan from aloe vera. *Industrial Crops and Products, 103*, 13–18. https://doi.org/10.1016/j.indcrop.2017.03.031

Sánchez, M., González-Burgos, E., Iglesias, I., & Gómez-Serranillos, M. P. (2020). Pharmacological update properties of aloe vera and its major active constituents. *Molecules (Basel, Switzerland), 25*(6), 1324. https://doi.org/10.3390/molecules25061324

Sharifiaghdam, M., Shaabani, E., Faridi-Majidi, R., De Smedt, S. C., Braeckmans, K., & Fraire, J. C. (2022). Macrophages as a therapeutic target to promote diabetic wound healing. *Molecular Therapy: The Journal of the American Society of Gene Therapy, 30*(9), 2891–2908. https://doi.org/10.1016/j.ymthe.2022.07.016

Sharma, S., Alfonso, A. R., Gordon, A. J., Kwong, J., Lin, L. J., & Chiu, E. S. (2022). Second-degree burns and aloe vera: A meta-analysis and systematic review. *Advances in Skin & Wound Care, 35*(11), 1–9. https://doi.org/10.1097/01.ASW.0000875056.29059.78

Silvestre-Roig, C., Fridlender, Z. G., Glogauer, M., & Scapini, P. (2019). Neutrophil diversity in health and disease. *Trends in Immunology, 40*(7), 565–583. https://doi.org/10.1016/j.it.2019.04.012

Su, W., Chang, Z., E, Y., Feng, Y., Yao, X., Wang, M., Ju, Y., Wang, K., Jiang, J., Li, P., & Lei, F. (2024). Electrospinning and electrospun polysaccharide-based nanofiber membranes: A review. *International Journal of Biological Macromolecules, 263*(Pt 2), Article 130335. https://doi.org/10.1016/j.ijbiomac.2024.130335

Summers, C., Rankin, S. M., Condliffe, A. M., Singh, N., Peters, A. M., & Chilvers, E. R. (2010). Neutrophil kinetics in health and disease. *Trends in Immunology, 31*(8), 318–324. https://doi.org/10.1016/j.it.2010.05.006

Tong, X., Li, M., Li, D., Lao, C., Chen, J., Xu, W., Du, J., Zhang, M., Yang, X., & Li, J. (2021a). Aloe vera gel extract: Safety evaluation for acute and chronic oral administration in sprague-dawley rats and anticancer activity in breast and lung cancer cells. *Journal of Ethnopharmacology, 280*, Article 114434. https://doi.org/10.1016/j.jep.2021.114434

Tong, X., Li, M., Li, D., Lao, C., Chen, J., Xu, W., Du, J., Zhang, M., Yang, X., & Li, J. (2021b). Aloe vera gel extract: Safety evaluation for acute and chronic oral administration in sprague-dawley rats and anticancer activity in breast and lung cancer cells. *Journal of Ethnopharmacology, 280*, Article 114434. https://doi.org/10.1016/j.jep.2021.114434

Tong, X., Li, M., Li, D., Lao, C., Chen, J., Xu, W., Du, J., Zhang, M., Yang, X., & Li, J. (2021c). Aloe vera gel extract: Safety evaluation for acute and chronic oral administration in sprague-dawley rats and anticancer activity in breast and lung cancer cells. *Journal of Ethnopharmacology, 280*, Article 114434. https://doi.org/10.1016/j.jep.2021.114434

Tornero-Martínez, A., Del, Carmen, Silva-Lucero, M., Sampedro, E. C., Ramón-Gallegos, E., Pérez-Cruz, C., Pérez-Grijalva, B., & Mora-Escobedo, R. (2022). Aloe vera and fermented extracts exhibit an anti-inflammatory effect on human glioblastoma/astrocytoma U373 MG cells. *Plant Foods for Human Nutrition (Dordrecht, Netherlands), 77*(1), 37–43. https://doi.org/10.1007/s11130-022-00957-4

V, V., B, Y. G., B, Z., S, K., G, İ., T, T., M, B., I, K., & Mr, S (2022). Polysaccharides in fabrication of membranes: A review. *Carbohydrate Polymers, 281*. https://doi.org/10.1016/j.carbpol.2021.119041

Wang, X., Wang, Z., Shen, M., Yi, C., Yu, Q., Chen, X., Xie, J., & Xie, M. (2024). Acetylated polysaccharides: Synthesis, physicochemical properties, bioactivities, and food applications. *Critical Reviews in Food Science and Nutrition, 64*(15), 4849–4864. https://doi.org/10.1080/10408398.2022.2146046

X, T., C, L., D, L., J, D., J, C., W, X., L, L., H, Y., X, G., & J, L (2022). An acetylated mannan isolated from aloe vera induce colorectal cancer cells apoptosis via mitochondrial pathway. *Carbohydrate Polymers, 291*. https://doi.org/10.1016/j.carbpol.2022.119464

Xing, W., Guo, W., Zou, C.-H., Fu, T.-T., Li, X.-Y., Zhu, M., Qi, J.-H., Song, J., Dong, C.-H., Li, Z., Xiao, Y., Yuan, P.-S., Huang, H., & Xu, X. (2015). Acemannan accelerates cell proliferation and skin wound healing through AKT/mTOR signaling pathway. *Journal of Dermatological Science, 79*(2), 101–109. https://doi.org/10.1016/j.jdermsci.2015.03.016

Zhang, Q., Zhang, M., Wang, T., Chen, X., Li, Q., & Zhao, X. (2022). Preparation of aloe polysaccharide/honey/PVA composite hydrogel: Antibacterial activity and promoting wound healing. *International Journal of Biological Macromolecules, 211*, 249–258. https://doi.org/10.1016/j.ijbiomac.2022.05.072